PERGAMON

International Journal of Solids and Structures 39 (2002) 1385–1403

INTERNATIONAL JOURNAL OF SOLIDS and STRUCTURES

www.elsevier.com/locate/ijsolstr

A new yield function and a hydrostatic stress-controlled void nucleation model for porous solids with pressure-sensitive matrices

H.-Y. Jeong *

Department of Mechanical Engineering, Sogang University, 1 Shinsoo-Dong, Mapo-Gu, Seoul 121-742, South Korea

Received 4 August 2000

Abstract

A macroscopic yield function for porous solids with pressure-sensitive matrices modeled by Coulomb's yield function was obtained by generalizing Gurson's yield function with consideration of the hydrostatic yield stress of a spherical thick-walled shell and by fitting the finite element results of the yield stresses of a voided cube. The macroscopic yield function is valid for the negative hydrostatic stress as well as for the positive hydrostatic stress. From the yield function, a plastic potential function for the porous solids was derived either for plastic normality flow or for plastic non-normality flow of the pressure-sensitive matrices. In addition, void nucleation was modeled by a normal distribution function with the macroscopic hydrostatic stress regarded as a controlling stress. This set of constitutive relations was implemented into a finite element code ABAQUS as a user material subroutine to analyze the cavitation and the deformation behavior of a rubber-modified epoxy around a crack tip under the Mode I plane strain conditions. By comparing the cavitation zone and the plastic zone obtained in the analysis with those observed in an experiment, the mean stress and the standard deviation for the void nucleation model could be determined. The cavitation and the deformation behavior of the rubber-modified epoxy were also analyzed around notches under four-point bending. The size and shape of the cavitation zone and the plastic zone were shown to be in good agreement with those observed in an experiment.

Keywords: Yield function; Porous solid; Void nucleation model; Rubber-modified epoxy

1. Introduction

In contrast to the classical plasticity theories, experiments showed that yielding of metals or polymers is dependent on the hydrostatic stress (Sternstein and Ongchin, 1969; Rabinowitz et al., 1970; Sauer et al., 1973; Spitzig et al., 1975, 1976; Spitzig and Richmond, 1979). The dependency of yielding on the hydrostatic stress, so called the pressure-sensitivity of yielding, has been modeled by Coulomb's yield function. In

* Fax: +82-2-712-0799.

E-mail address: jeonghy@sogang.ac.kr (H.-Y. Jeong).

0020-7683/02/$ - see front matter
PII: S0020-7683(01)00260-8

addition, if there exist microvoids or soft inclusions even in a solid (matrix) which does not show any pressure-sensitivity of yielding, the macroscopic yielding of the solid becomes pressure-sensitive. Taking into account the macroscopic pressure-sensitivity of yielding, Gurson (1975, 1977) developed a yield function for porous solids.

It has been well known that some brittle polymers can be toughened by adding rubber particles. For example, rubber-modified epoxies are 10 times or more tougher than epoxy resins (Yee and Pearson, 1986; Pearson and Yee, 1986, 1991). Yee and his colleagues (Yee and Pearson, 1986; Pearson and Yee, 1986, 1991; Yee et al., 1993) showed that as a rubber-modified epoxy deforms, rubber particles cavitate and massive shear yielding occurs subsequently around the cavitated rubber particles, and this massive shear yielding is the major toughening mechanism. The cavitation which plays a key role in the toughening process can be considered as void nucleation occurring in the composite material of the epoxy matrix and rubber particles. In addition, in order to analyze the plastic deformation of the composite material it is necessary to take into account both the pressure-sensitivity of the matrix and the macroscopic pressure-sensitivity of the composite material due to nucleated voids.

The author (1992; Jeong and Pan, 1995) developed a yield function for porous solids with pressure sensitive matrices, and used the yield function to analyze the cavitation and the plastic deformation of a rubber-modified epoxy around a crack tip. The author regarded cavitation as void nucleation controlled by the sum of the matrix flow stress and the macroscopic hydrostatic stress. Lazzeri and Bucknall (1993) also developed a different yield function for porous solids with pressure-sensitive matrices, and they used their yield function to show that the shear band formed under plane strain deformation rotates toward the perpendicular direction to the major principal stress direction as the void volume fraction increases. Al-Abduljabbar and Pan (1999) noted experimental results (Pearson and Yee, 1986, 1991; Yee et al., 1993) that rubber particles in a rubber-modified epoxy cavitate only under the positive hydrostatic stress, and the particles start to cavitate before noticeable plastic deformation. They also argued that a rubber-modified epoxy under the positive hydrostatic stress can be regarded as a porous solid, but under the negative hydrostatic stress it can be regarded as a non-porous solid. Therefore, in the analysis of the material behavior of a rubber-modified epoxy around notches under four-point bending they used the yield function developed by the author (1992; Jeong and Pan, 1995) for the positive hydrostatic stress, but they used a linear yield function of Coulomb's yield function type for the negative hydrostatic stress.

It is noteworthy that even though the yield functions proposed by the author (1992; Jeong and Pan, 1995), Lazzeri and Bucknall (1993), and Al-Abduljabbar and Pan (1999) were successfully used in each analysis mentioned above, the yield functions cannot be applied to porous solids with pressure-sensitive matrices under the negative hydrostatic stress. The yield functions developed by the author (1992; Jeong and Pan, 1995), and Lazzeri and Bucknall (1993) are not defined for the negative hydrostatic stress. The linear yield function proposed by Al-Abduljabbar and Pan (1999) is valid for a rubber-modified epoxy in which rubber particles do not cavitate under the negative hydrostatic stress, but it is not valid for porous solids under the negative hydrostatic stress. Therefore, in this paper a new yield function, which is valid for the negative hydrostatic stress as well as for the positive hydrostatic stress, was developed for porous solids with pressure-sensitive matrices. From the yield function, a plastic potential function for the porous solids was derived either for plastic normality flow or for plastic non-normality flow of pressure-sensitive matrices.

In addition to the new yield function and the plastic potential function, elastic relations, an evolution rule of the flow stress of the matrices, a consistency equation, a void nucleation model and a void volume evolution equation were presented to complete a set of constitutive relations. The set of constitutive relations was implemented into a finite element code ABAQUS as a user material subroutine. By using the user subroutine, the cavitation and the deformation behavior of a rubber-modified epoxy (DER331/Pip/CTBN-8(10)) were analyzed around a crack tip under the Mode I plane strain conditions, and they were also

analyzed around notches under four-point bending. Unlike Al-Abduljabbar and Pan (1999) who regarded rubber particles as voids from the very beginning of deformation and ignored cavitation, the author regarded cavitation as void nucleation occurring in the rubber-modified epoxy.

In order to mathematically represent void nucleation, a normal distribution function was proposed to use by Chu and Needleman (1980). Since then, two models have been used; one is the stress-controlled void nucleation model, and the other is the plastic strain-controlled void nucleation model. For the stress-controlled void nucleation model the sum of the tensile flow stress and the macroscopic hydrostatic stress was used as a controlling stress in many researches (e.g. Tvergaard, 1982b; Pan et al., 1983; Needleman and Tvergaard, 1987; Jeong, 1992; Jeong and Pan, 1995, 1996). The sum was suggested to be an approximation to the maximum stress transmitted across the particle–matrix interface, and void nucleation was believed to depend on the sum (Argon and Im, 1975). In this paper this void nucleation model is named the maximum stress-controlled void nucleation model. However, it is noteworthy that several experiments showed circular cavitation zones around a crack tip in rubber-modified epoxies (Pearson and Yee, 1991; Yee et al., 1993), and the shape of the cavitation zones is similar to that of the contour plots of the macroscopic hydrostatic stress. In addition, Lazzeri and Bucknall (1993, 2000) derived an equation for a critical volumetric strain required to cause cavitation, and they showed that the critical volumetric strain was in good agreement with experimental results. Thus, it is appropriate to use the macroscopic hydrostatic stress as a controlling stress in modeling the void nucleation (cavitation) process. This void nucleation model is named the hydrostatic stress-controlled void nucleation model.

The void nucleation models of the normal distribution function type have three material constants to be determined: the volume fraction of void nucleating particles, the standard deviation and the mean value. Since the volume fraction of void nucleating particles in a rubber-modified epoxy is equal to that of rubber particles, it can be easily determined. However, the other two constants cannot be easily determined. In many researches using one of the void nucleation models (e.g., Chu and Needleman, 1980; Pan et al., 1983; Jeong and Pan, 1995, 1996), the standard deviation and the mean value were somewhat arbitrarily determined, and their effects were analyzed by conducting a parametric study.

However, in this paper the standard deviation and the mean value used in the hydrostatic stress-controlled void nucleation model were determined by comparing the simulation results of the material behavior around a crack tip with experimental results. From the asymptotic solutions of the stress field around a crack tip under the Mode I plane strain conditions, the contour plots of the macroscopic hydrostatic stress can be obtained. By comparing the contour plots with the circular cavitation zone observed in an experiment, the hydrostatic stress causing cavitation could be determined. Then, the standard deviation and the mean value were selected in a way that the integral of the hydrostatic stress-controlled void nucleation model from the zero hydrostatic stress to the hydrostatic stress causing cavitation was equal to the void volume fraction at the edge of the cavitation zone. In other words, when one of the two constants was selected, the other was fixed. However, there were still numerous sets of the standard deviation and the mean value satisfying the above-mentioned requirement. Thus, the effect of the standard deviation and the mean value on the size of the cavitation zone and the plastic zone (or the massive cavitation zone) was analyzed. The analysis showed that as the mean value increased, the cavitation zone and the plastic zone became smaller. Finally, a set of the standard deviation and the mean value which resulted in the comparable size and shape of the cavitation zone and the plastic zone to those observed in an experiment could be determined.

By using the hydrostatic stress-controlled void nucleation model with the mean value and the standard deviation determined in the above-mentioned manner, the material behavior of the rubber-modified epoxy (DER331/Pip/CTBN-8(10)) was also analyzed around the notches in a symmetric double-edge double-notched (SDEDN) specimen under four-point bending. The numerical analysis showed that no cavitation occurred around the notch under compression, but a circular cavitation zone formed around the notch

under tension. It also showed that the plastic deformation occurred in a limited area around the notch under compression, but the plastic deformation occurred in a comparatively large area around the notch under tension. These numerical results were in good agreement with the corresponding experimental results.

2. Constitutive law

2.1. New yield function for porous solids with pressure-sensitive matrices

The pressure-sensitivity of yielding of steels or polymers has been modeled by Coulomb's yield function in which yielding is assumed to occur when a linear combination of the effective stress and the hydrostatic stress reaches the flow stress (Sternstein and Ongchin, 1969; Spitzig and Richmond, 1979; Kinloch and Young, 1983), and the yield function is given as

$$\tau_e + \mu\sigma_m = \tau_o \quad \text{or} \quad \sigma_e + \mu'\sigma_m = \sigma_o \tag{1}$$

Here, τ_e is the effective shear stress, μ is the pressure-sensitivity factor, σ_m is the hydrostatic stress, τ_o is the shear flow stress, σ_e is the effective stress, μ' is $\sqrt{3}\mu$, and σ_o is $\sqrt{3}\tau_o$. Note here that σ_o is not the tensile flow stress but the sum of the tensile flow stress and μ' times one third of it. Experiments showed that the pressure-sensitivity factor ranges from 0.014 to 0.064 for steels (Spitzig et al., 1975, 1976), and from 0.10 to 0.25 for polymers (Kinloch and Young, 1983). Moreover, the phase transformation of zirconia-containing ceramics can be also modeled by Coulomb's yield function, and the pressure-sensitivity factor for the phase transformation ranges from 0.55 to 0.93 (Yu and Shetty, 1989; Chen, 1991).

Gurson (1975, 1977) assumed a porous solid to have a periodic array of voids and to be an assembly of identical spherical shells with voids at the center. He also assumed the matrix to be pressure-insensitive, i.e. a von Mises material. Utilizing the upper bound approach for the spherical shell, Gurson (1975, 1977) developed a yield function for the porous solid as follows.

$$\Phi_G(\boldsymbol{\Sigma}, \sigma_o, f) = \left(\frac{\Sigma_e}{\sigma_o}\right)^2 + 2f\cosh\left(\frac{3\Sigma_m}{2\sigma_o}\right) - 1 - f^2 = 0 \tag{2}$$

Here, $\boldsymbol{\Sigma}$ is the macroscopic Cauchy stress exerting on the porous solid, Σ_e is the macroscopic effective stress, Σ_m is the macroscopic hydrostatic stress, and f is the void volume fraction of the porous solid.

However, it is difficult to find a kinematically admissible velocity field for the spherical shell with the pressure-sensitive matrix modeled by Coulomb's yield function, and the upper bound approach cannot be used. Instead, the hydrostatic yield stress can be found, using the equilibrium equation and Coulomb's yield function, i.e. the lower bound approach, and it is given as

$$(\Sigma_m)_y = \frac{\sigma_o}{\mu'}\left\{1 - f^{\left(\pm 2\mu'/(3\pm 2\mu')\right)}\right\} \tag{3}$$

The positive sign in the exponent in Eq. (3) gives the positive hydrostatic yield stress, and the negative sign gives the negative hydrostatic yield stress. Note that the absolute value of the negative hydrostatic yield stress is always bigger than the positive hydrostatic yield stress. It can be proven from Eq. (3) that $(\Sigma_m)_y$ approaches $\pm(2/3)\sigma_o \log f$ as μ approaches 0. That is, $2f\cosh(3\Sigma_m/2\sigma_o)$ approaches $1 + f^2$, and Gurson's yield function is satisfied. However, when μ is not equal to 0, $2f\cosh\{(3 + \text{sign}(\Sigma_m)2\mu')/(2\mu')\log(1 - \mu'(\Sigma_m/\sigma_o))\}$ becomes equal to $1 + f^2$. In addition, a yield function for porous solids with pressure-sensitive matrices should reduce to Gurson's yield function when μ is equal to 0, and it should reduce to Coulomb's yield function when f is equal to 0. Based on these requirements, a yield function could be proposed as follows.

$$\Phi_{\mathrm{I}}(\boldsymbol{\Sigma},\sigma_{\mathrm{o}},f,\mu')=\left(\frac{\Sigma_{\mathrm{e}}}{\sigma_{\mathrm{o}}}\right)^2+\left(1-\mu'\frac{\Sigma_{\mathrm{m}}}{\sigma_{\mathrm{o}}}\right)^2\left[2f\cosh\left\{\frac{3+\mathrm{sign}(\Sigma_{\mathrm{m}})2\mu'}{2\mu'}\log\left(1-\mu'\frac{\Sigma_{\mathrm{m}}}{\sigma_{\mathrm{o}}}\right)\right\}-1-f^2\right]=0 \tag{4}$$

When $\Sigma_{\mathrm{e}}=0$, Eq. (4) results in $(\Sigma_{\mathrm{m}})_{\mathrm{y}}$ given in Eq. (3). In addition, as μ (or μ') approaches 0, Eq. (4) reduces to Eq. (2). When f becomes zero, Eq. (4) reduces to Eq. (1). Thus, the yield function in Eq. (4) satisfies the above-mentioned requirements.

Meanwhile, the author (1992; Jeong and Pan, 1995) proposed a yield function for porous solids with pressure-sensitive matrices as follows, and successfully used the yield function to analyze the material behavior of a rubber-modified epoxy around a crack tip under the Mode I plane strain conditions.

$$\Phi_{\mathrm{J}}(\boldsymbol{\Sigma},\sigma_{\mathrm{o}},f,\mu')=\left(\frac{\Sigma_{\mathrm{e}}+\mu'\Sigma_{\mathrm{m}}}{\sigma_{\mathrm{o}}}\right)^2+2f\cosh\left[\frac{3+\mu'}{2\mu'}\log\left(1-\mu'\frac{\Sigma_{\mathrm{m}}}{\sigma_{\mathrm{o}}}\right)\right]-1-f^2=0 \tag{5}$$

However, when Σ_{m} becomes very negative, any positive Σ_{e} satisfying Eq. (5) does not exist. That is, the yield function is not defined for the negative hydrostatic stress. Lazzeri and Bucknall (1993) also proposed a different yield function for porous solids with pressure matrices, and they successfully used their yield function to calculate the angle of the shear band formed in a rubber-modified polymer under plane strain deformation. However, their yield function is not defined for the negative hydrostatic stress, either. Al-Abduljabbar and Pan (1999) used the yield function in Eq. (5) for the positive hydrostatic stress, but they defined a linear yield function of Coulomb's yield function type for the negative hydrostatic stress such that at the zero hydrostatic stress it is continuous to the yield function in Eq. (5). The yield function Al-Abduljabbar and Pan (1999) defined is given as follows.

$$\Phi_{\mathrm{A}}(\boldsymbol{\Sigma},\sigma_{\mathrm{o}},f,\mu')=\left(\frac{\Sigma_{\mathrm{e}}+\mu'\Sigma_{\mathrm{m}}}{\sigma_{\mathrm{o}}}\right)^2+2f-1-f^2=0 \tag{6}$$

Actually, the author (1992; Jeong and Pan, 1995), and Al-Abduljabbar and Pan (1999) incorporated three parameters, which will be explained in the next section, in their yield functions, but the parameters are not shown for the sake of brevity. Al-Abduljabbar and Pan (1999) successfully used the linear yield function in Eq. (6) to analyze the material behavior of a rubber-modified epoxy because rubber particles do not cavitate under the negative hydrostatic stress. Note that the effective stress satisfying Eq. (6) increases linearly as the negative hydrostatic stress increases when μ is not equal to 0, and it remains constant regardless of the hydrostatic stress when μ is equal to 0. That is, the yield function in Eq. (6) does not become equal to Gurson's yield function when μ is equal to 0. Therefore, it can be said that even though the yield function in Eq. (6) can be applied to a rubber-modified epoxy with no cavitation under the negative hydrostatic stress, it cannot be applied to porous solids with pressure-sensitive matrices under the negative hydrostatic stress. However, the yield function in Eq. (4) can be applied to porous solids with pressure-sensitive matrices under the negative hydrostatic stress as well as under the positive hydrostatic stress.

2.2. Interaction between voids

The yield function in Eq. (2) was obtained with no consideration of interaction between voids, and so was the yield function in Eq. (4). This results from the fact that Gurson (1975, 1977) assumed a porous solid to be an assembly of spherical shells, leaving space between them. Actually, in order to take into account the interaction, it is necessary to adopt a voided cube instead of a spherical shell as shown in Fig. 1. Since it is impossible to obtain analytically the yield stresses of a voided cube, the finite element method was used for a voided cube with the matrix assumed to be almost rigid-perfectly plastic ($E/\sigma_{\mathrm{o}}=2\times10^9$). The cube being subject to axisymmetric loading, the macroscopic hydrostatic stress and the macroscopic effective stress

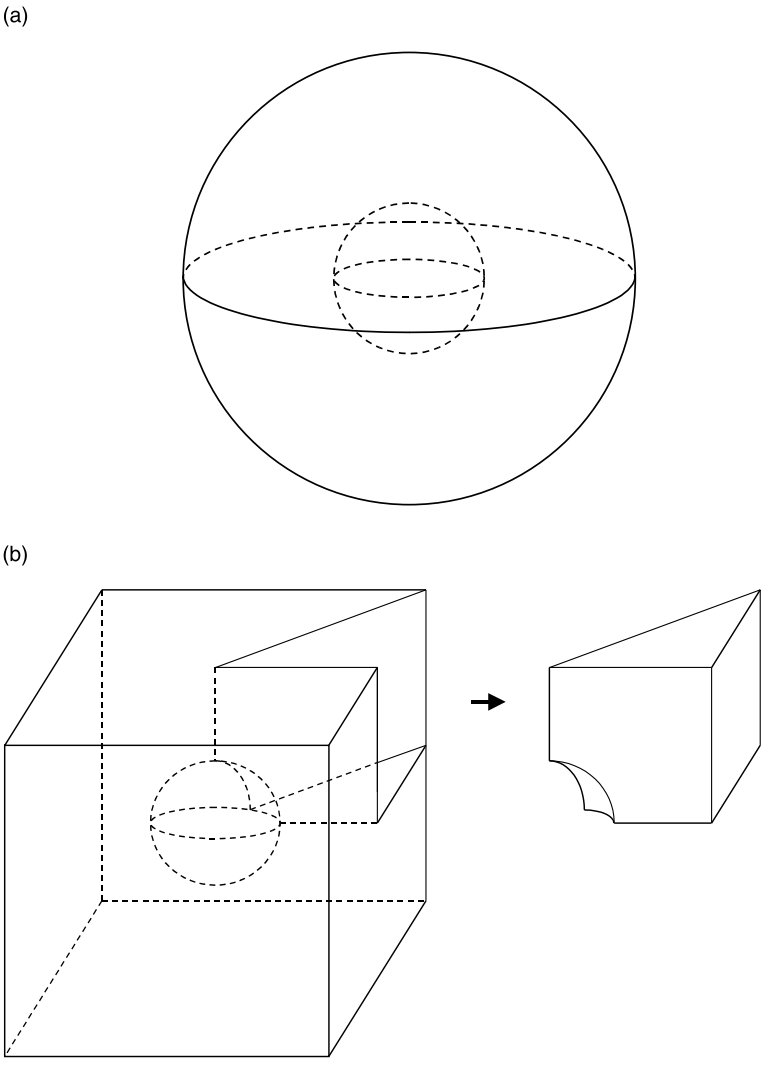

Fig. 1. (a) A spherical thick-walled shell model. (b) A voided cube model.

were obtained when massive plastic deformation occurred in the cube. The macroscopic stress invariants were plotted as empty symbols in Fig. 2 after being normalized by σ_o. As expected, the macroscopic stress invariants were located inside the loci defined by Eq. (4) (the loci shown in Fig. 2 were obtained from Eq. (7)). This means that the interaction between voids helps the porous solid yield at lower loads. In order to fit better the FEM results, three parameters ($q_1 = 1.35$, $q_2 = 0.95$, $q_3 = 1.35$) proposed by the author (1992) were incorporated in Eq. (4) as follows.

$$\Phi_y(\boldsymbol{\Sigma}, \sigma_o, f, \mu') = \left(\frac{\Sigma_e}{\sigma_o}\right)^2 + \left(1 - \mu'\frac{\Sigma_m}{\sigma_o}\right)^2 \times \left[2q_1 f \cosh\left\{q_2 \frac{3 + \mathrm{sign}(\Sigma_m)2\mu'}{2\mu'} \log\left(1 - \mu'\frac{\Sigma_m}{\sigma_o}\right)\right\} - 1 - q_3 f^2\right] = 0 \tag{7}$$

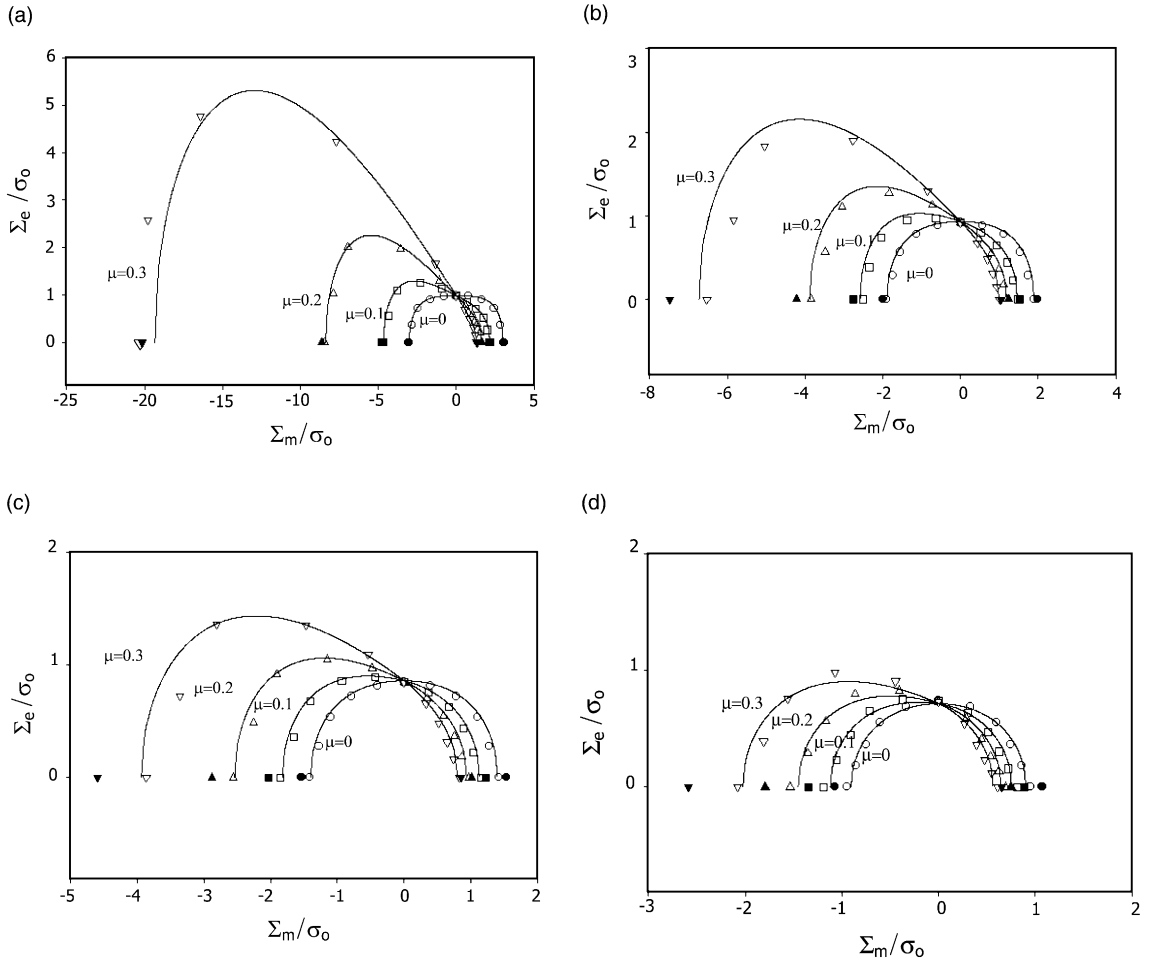

Fig. 2. (a) The yield function Φ_y, FEM results and $(\Sigma_m)_y$ for $f = 0.01$. (b) The yield function Φ_y, FEM results and $(\Sigma_m)_y$ for $f = 0.05$. (c) The yield function Φ_y, FEM results and $(\Sigma_m)_y$ for $f = 0.10$. (d) The yield function Φ_y, FEM results and $(\Sigma_m)_y$ for $f = 0.20$.

Note that Tvergaard (1981, 1982a) introduced different values of parameters ($q_1 = 1.5$, $q_2 = 1.0$, $q_3 = 2.25$) into Gurson's yield function after comparing the plastic flow localization results of his finite element computations with those of a continuum model based on Gurson's yield function.

2.3. Modified yield function, FEM results and hydrostatic yield stresses

In Fig. 2(a)–(d), the yield function Φ_y (curves) along with the FEM results (empty symbols) and the hydrostatic yield stresses $(\Sigma_m)_y$ (solid symbols) are shown for four different void volume fractions and four different pressure-sensitivity factors. It is noteworthy that the yield function Φ_y correlates well with the FEM results for a wide range of the void volume fraction, the pressure-sensitivity factor and the hydrostatic stress. The FEM results clearly show that a porous solid yields under hydrostatic pressure, and it yields at higher hydrostatic pressure as μ increases. The difference between the solid symbols and the empty symbols located on the abscissa indicates the effect of interaction between voids on yielding. As shown in Fig. 2(a)–(d), the effect increases as f or μ increases, especially for the negative hydrostatic stress.

2.4. Plastic potential function

Experiments showed that during plastic deformation steels or polymers modeled by Coulomb's yield function dilate less than is predicted by the normality plastic flow rule (Spitzig et al., 1975, 1976; Spitzig and Richmond, 1979). This means that the plastic potential function is not the same as the yield function. If the dilatancy factor is denoted by β and the effective shear plastic strain is denoted by γ_e^p, the volume increase of the pressure-sensitive matrix during plastic deformation can be expressed as $\beta\gamma_e^p$, and the plastic potential function of the matrix can be defined as follows.

$$\tau_e + \beta\sigma_m = \tau_p \tag{8}$$

Note that the plastic potential function is the same as Coulomb's yield function if μ and τ_o are replaced by β and τ_p, respectively. Here, τ_p is the fictitious shear flow stress that makes the current stress state satisfy Eq. (8). Gurson (1975) proved that if the matrix satisfies the normality flow rule, the porous solid also satisfies it. This means that if the plastic flow of the matrix is normal to Eq. (1), the plastic flow of the porous solid is normal to Eq. (7). By the same token, if the plastic flow of the matrix is normal to Eq. (8), the plastic flow of the porous solid is normal to the plastic potential function $\Phi_p(\boldsymbol{\Sigma}, \sigma_p, f, \beta') = 0$, which can be obtained from the yield function $\Phi_y(\boldsymbol{\Sigma}, \sigma_o, f, \mu') = 0$ by replacing μ' and σ_o by β' $(= \sqrt{3}\beta)$ and σ_p, respectively. Here, σ_p is the fictitious flow stress that makes the current stress state satisfy $\Phi_p(\boldsymbol{\Sigma}, \sigma_p, f, \beta') = 0$. Note that only when μ (or μ') is equal to β (or β'), the plastic potential function becomes the same as the yield function, and plastic normality flow occurs.

2.5. Elastic relations

When the void volume fraction is large, its effect on the elastic moduli of a porous solid should be taken into account. Adopting the self-consistent scheme combined with the average stress scheme (Tandon and Weng, 1988), Young's modulus E^* and Poisson's ratio v^* of a porous solid could be calculated from those of the matrix, E and v, and the void volume fraction f as follows.

$$E^* = \frac{2E(7-5v)(1-f)}{14-10v+f(1+v)(13-15v)} \tag{9}$$

$$v^* = \frac{v(14-10v)+f(1+v)(3-5v)}{14-10v+f(1+v)(13-15v)} \tag{10}$$

In modeling a rubber-modified epoxy of this paper f is the volume fraction of cavitated voids, E, v and E^*, v^* are elastic moduli of the composite before and after cavitation, respectively.

2.6. Void nucleation models and void volume evolution equation

The increase of void volume arises both from the growth of existing voids and from the nucleation of voids. As for the nucleation of voids, two models have been used; one is the stress-controlled void nucleation model, and the other is the plastic strain-controlled void nucleation model. As for the stress-controlled void nucleation model, the sum of the tensile flow stress and the macroscopic hydrostatic stress was used as a controlling stress in many researches (e.g., Tvergaard, 1982b; Pan et al., 1983; Needleman and Tvergaard, 1987; Jeong, 1992; Jeong and Pan, 1995, 1996). The sum was suggested to be an approximation to the maximum stress transmitted across the particle–matrix interface, and void nucleation was believed to depend on the maximum stress (Argon and Im, 1975). In this paper this void nucleation model is named the maximum stress-controlled void nucleation model. Some experiments showed circular cavitation zones around a crack tip in rubber-modified epoxies under the Mode I plane strain conditions (Pearson and Yee,

1991), and the shape of the cavitation zones is similar to that of the contour plots of the macroscopic hydrostatic stress. In addition, Lazzeri and Bucknall (1993, 2000) derived an equation for a critical volumetric strain required to cause cavitation, and they showed that the critical volumetric strain was in good agreement with experimental results. With the assumption of linear elasticity for rubber particles, the critical volumetric strain multiplied by the bulk modulus of the rubber particles results in the critical hydrostatic stress required to cause cavitation. Thus, it is meaningful to investigate if the macroscopic hydrostatic stress can be used as a controlling stress in modeling the void nucleation (cavitation) process. This void nucleation model is named the hydrostatic stress-controlled void nucleation model.

Therefore, the void volume evolution equation can be expressed as follows.

$$\dot{f} = (1-f)[\mathrm{tr}(\mathbf{D}^{\mathrm{p}}) - \beta'\dot{\varepsilon}_{\mathrm{e}}^{\mathrm{p}}] + A\dot{\sigma}_{\mathrm{o}} + B\dot{\Sigma}_{\mathrm{m}} + C\dot{\varepsilon}_{\mathrm{e}}^{\mathrm{p}} \tag{11}$$

Here, the first term at the right side represents the void volume increase due to void growth, and the last three terms represent the void volume increase due to void nucleation. In addition, $\mathrm{tr}(\mathbf{D}^{\mathrm{p}})$ is the trace of the rate-of-deformation tensor, and $\dot{\varepsilon}_{\mathrm{e}}^{\mathrm{p}}$ is the effective plastic strain rate. For the maximum stress-controlled void nucleation model,

$$A = B = \frac{f_{\mathrm{N}}}{s\sigma_{\mathrm{y}}\sqrt{2\pi}} \exp\left[-\frac{1}{2}\left(\frac{\sigma_{\mathrm{o}} + \Sigma_{\mathrm{m}} - \sigma_{\mathrm{N}}}{s\sigma_{\mathrm{y}}}\right)^2\right], \quad C = 0 \tag{12}$$

However, for the hydrostatic stress-controlled void nucleation model,

$$A = 0, \quad B = \frac{f_{\mathrm{N}}}{s\sigma_{\mathrm{y}}\sqrt{2\pi}} \exp\left[-\frac{1}{2}\left(\frac{\Sigma_{\mathrm{m}} - \sigma_{\mathrm{N}}}{s\sigma_{\mathrm{y}}}\right)^2\right], \quad C = 0 \tag{13}$$

Finally, for the plastic strain-controlled void nucleation model,

$$A = B = 0, \quad C = \frac{f_{\mathrm{N}}}{s\sqrt{2\pi}} \exp\left[-\frac{1}{2}\left(\frac{\varepsilon_{\mathrm{e}}^{\mathrm{p}} - \varepsilon_{\mathrm{N}}}{s}\right)^2\right] \tag{14}$$

Here, f_{N} is the volume fraction of void nucleating particles, s and σ_{N} (or ε_{N}) are the standard deviation and the mean value of the normal distribution function, respectively. In addition, A, B and C are set to zero unless the controlling stress (or the controlling strain) is bigger than zero and its maximum value which occurred in the previous deformation history. For example, when the macroscopic hydrostatic stress remains negative through a deformation history, the hydrostatic stress-controlled void nucleation model does not result in any void nucleation.

2.7. Strain rate sensitivity and strain softening-and-hardening

Some polymers show initial intrinsic strain softening and subsequent hardening (Haward, 1973) as well as strain rate sensitivity (Bowden, 1973; Yee and Pearson, 1986). A simple power law with the strain rate hardening exponent m was adopted as follows.

$$\dot{\varepsilon}_{\mathrm{e}}^{\mathrm{p}} = \dot{\varepsilon}_{\mathrm{r}}\left[\frac{\sigma_{\mathrm{o}}}{g(\varepsilon_{\mathrm{e}}^{\mathrm{p}})}\right]^{1/m} \tag{15}$$

Here, $\dot{\varepsilon}_{\mathrm{r}}$ is the reference tensile plastic strain rate, and the function $g(\varepsilon_{\mathrm{e}}^{\mathrm{p}})$ equals the flow stress σ_{o} of the matrix when $\dot{\varepsilon}_{\mathrm{e}}^{\mathrm{p}} = \dot{\varepsilon}_{\mathrm{r}}$. If $\dot{\varepsilon}_{\mathrm{e}}^{\mathrm{p}}$ is greater (or smaller) than $\dot{\varepsilon}_{\mathrm{r}}$, σ_{o} becomes greater (or smaller) than $g(\varepsilon_{\mathrm{e}}^{\mathrm{p}})$. To model qualitatively the initial strain softening and subsequent hardening behavior of epoxies, a function for $g(\varepsilon_{\mathrm{e}}^{\mathrm{p}})$ was proposed as follows.

$$g(\varepsilon_e^p) = \sigma_y \left[\left(\frac{\varepsilon_e^p}{\varepsilon_y} + 1 \right)^N + C_1 \left(\frac{\varepsilon_e^p}{\varepsilon_y} \right)^{N_1} \log \left(C_2 \frac{\varepsilon_e^p}{\varepsilon_y} \right) \right] \tag{16}$$

Here, N is the hardening exponent, N_1 is a softening–hardening exponent, and C_1 and C_2 are two material coefficients. In addition, σ_y is equal to $\sqrt{3}\tau_y$, where τ_y is the shear yield stress obtained at the reference shear plastic strain rate $\dot{\gamma}_r$ $(= \sqrt{3}\dot{\varepsilon}_r)$, and ε_y is σ_y/E. Note here that σ_o is equal to σ_y when $\varepsilon_e^p = 0$ and $\dot{\varepsilon}_e^p = \dot{\varepsilon}_r$. When C_1 is equal to zero, Eq. (16) reduces to the usual power-law strain hardening equation.

For detailed derivations of the constitutive relations except the new yield function and the hydrostatic stress-controlled void nucleation model, refer to the author's previous papers (Jeong, 1992; Jeong and Pan, 1995).

3. Material behavior of a rubber-modified epoxy

3.1. Finite element models

The set of constitutive relations developed in the previous sections was implemented into ABAQUS as a user material subroutine. This subroutine was used to analyze the material behavior of a rubber-modified epoxy (DER331/Pip/CTBN-8(10)) around a crack and around double notches. Pearson and Yee (1986, 1991) conducted a four-point bending test on a double-cracked specimen to capture the material behavior just prior to final failure under the Mode I plane strain conditions. In addition, Yee et al. (1993) conducted a four-point bending test on an SDEDN specimen to investigate the material behavior around a notch under tension and around the other notch under compression prior to final failure.

Due to symmetry, only the upper half around a crack under the Mode I plane strain loading was discretized to create inner and outer meshes as shown in Fig. 3(a) and (b). The outer radius of the outer mesh was 10,000 times bigger than the crack-tip radius, and the small-scale yielding conditions were guaranteed. In addition, an SDEDN specimen under four-point bending was discretized only for the left half as shown in Fig. 4. The arrow represents the loading direction along which the bending crosshead moved at a rate of 1 mm/min. Note that the material around the upper notch was under compression, and the material around the lower notch was under tension.

The material properties of the rubber-modified epoxy analyzed in this paper are $E = 2530$ MPa, $v = 0.428$, $\sigma_y = 75$ MPa, $m = 0.035$, $N = 0.1$, $N_1 = 1.3$, $C_1 = 0.03$, $C_2 = 0.05$, $\dot{\varepsilon}_r = 0.0032$/sec, $\mu = 0.13$,

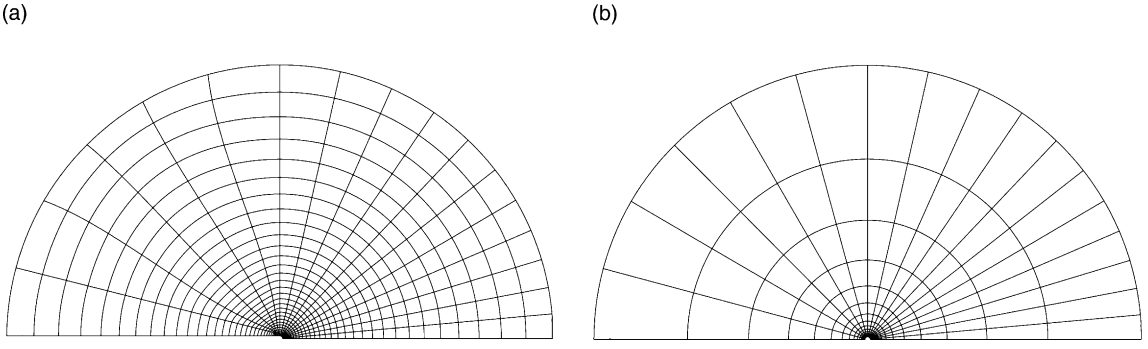

Fig. 3. (a) Inner mesh around a crack under the Mode I plane strain conditions. (b) Outer mesh around a crack under the Mode I plane strain conditions.

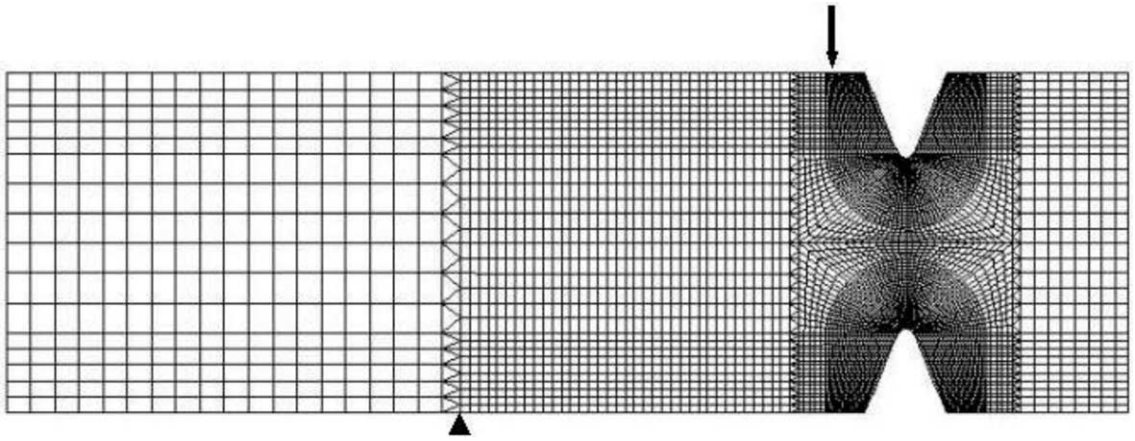

Fig. 4. FEM mesh for the SDEDN specimen.

$\beta = 0$, and $f_N = 0.12$. These material properties were obtained mainly from the experimental results (Yee and Pearson, 1986; Pearson and Yee, 1986). Note that during a simple shear test the hydrostatic stress remains zero, and no cavitation occurs. In addition, σ_o is equal to σ_y when $\varepsilon_e^p = 0$ and $\dot{\varepsilon}_e^p = \dot{\varepsilon}_r$, and σ_y can be obtained from the shear yield stress as provided by $\sigma_y = \sqrt{3}\tau_y$. However, since there was no shear yield stress available for the rubber-modified epoxy (DER331/Pip/CTBN-8(10)), by using Eq. (1) σ_y was calculated from the tensile yield stress of the rubber-modified epoxy, which is about 70 MPa at $\dot{\varepsilon}_r = 0.0032$/sec (see Fig. 16 in Yee and Pearson, 1986).

$$\sigma_y = 70 + 0.13 \times \sqrt{3} \times 70/3 \cong 75 \text{ MPa} \tag{17}$$

Al-Abduljabbar and Pan (1999) considered rubber particles as voids from the very beginning of the deformation history, and they ignored the cavitation process. Thus, they used σ_y of the pure epoxy, and took into account the reduction in σ_y due to addition of rubber particles by incorporating f of which the initial value was equal to the volume fraction of rubber particles. It can be easily proven from Eqs. (4), (6) or (7) that σ_y is reduced by a factor of $1 - f$ or $(1 - 2q_1 f + q_3 f^2)^{1/2}$. Regarding rubber particles as voids, the yield function in Eq. (7) was plotted along with experimental data of Kody and Lesser (1998) in Fig. 5. Note that there is a noticeable difference between the yield function and the experimental data especially when the volume fraction of rubber particles is large, and a similar amount of difference exists in the case of the yield functions proposed by the author (1992; Jeong and Pan, 1995), and Al-Abduljabbar and Pan (1999). As Kody and Lesser (1998) pointed out, there exists a bigger difference between the yield function proposed by Lazzeri and Bucknall (1993) and the experimental data. However, a bigger difference mainly results from the fact that there are no correction parameters such as q_1, q_2 and q_3 included in the yield function. For the analysis of this paper σ_y of the rubber-modified epoxy could have been approximated by reducing that of the pure epoxy by a factor of $(1 - 2q_1 f + q_3 f^2)^{1/2}$, but it was calculated from the tensile yield stress of the rubber-modified epoxy as in Eq. (17). Note again that in the analyses of this paper f is the volume fraction of cavitated voids, which remains zero under the negative hydrostatic stress. When f is equal to zero, the yield function in Eq. (7) becomes equal to Coulomb's yield function, the correction parameters being ignored. Therefore, for the analyses of this paper σ_y should represent the initial flow stress of the rubber-modified epoxy, not that of the pure epoxy.

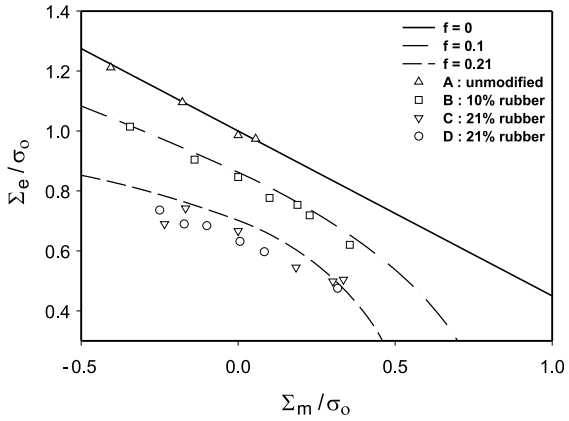

Fig. 5. The comparison of the yield function Φ_y with the test data (Kody and Lesser, 1998), regarding rubber particles as voids.

3.2. Cavitation zone and hydrostatic stress contour

Pearson and Yee (1991) obtained optical microscopies of the rubber-modified epoxy at the mid-plane near the crack tip. Shown in Fig. 6 was a typical microscopy obtained with the critical stress intensity factor K_{IC} equal to 2.1 MPa $\sqrt{m}$. Here, the plastic zone is baseball-bat shaped, formed along the crack line, and the length of the plastic zone is about 600 μm. The cavitation zone is circular, surrounding the plastic zone, and the diameter of the cavitation zone is about 1600 μm. It is noteworthy that rubber particles in the plastic zone were massively cavitated. Based on these findings, Pearson and Yee (1991) claimed that rubber particles became cavitated before noticeable plastic deformation occurred, and the rubber cavitation relieved the hydrostatic stress, helping the epoxy matrix deform plastically. Thus, they concluded that the massive plastic deformation was the major toughening mechanism of the rubber-modified epoxy.

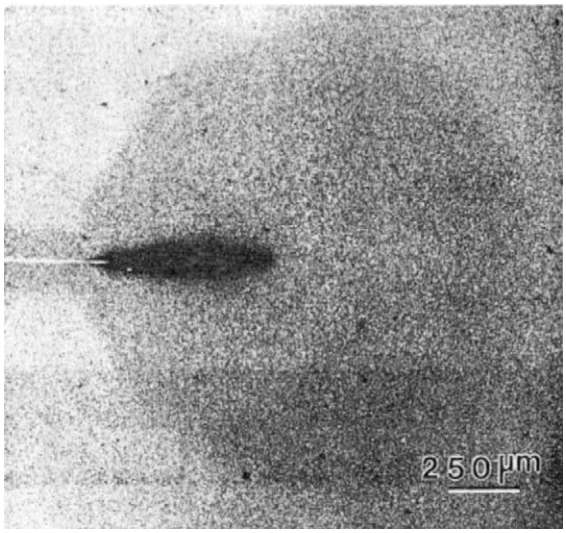

Fig. 6. Optical micrograph of a thin section taken at the mid-plane near the crack tip in the rubber-modified epoxy (from Pearson and Yee, 1991).

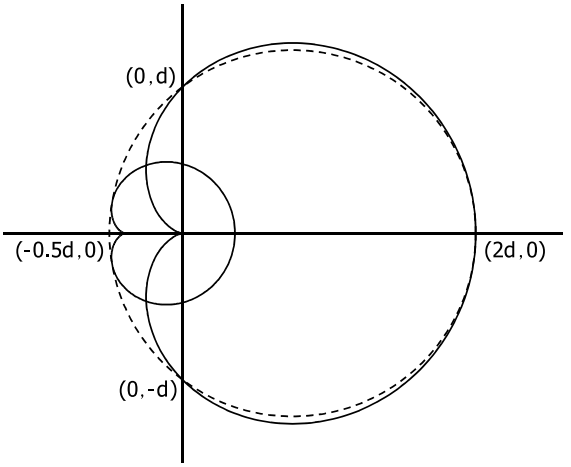

Fig. 7. Contour plots of the hydrostatic stress and a circle crossing the same intersections.

From the asymptotic solutions of stress fields around a crack tip under the Mode I plane strain conditions, the contour plot of the hydrostatic stress can be expressed in the polar coordinates as follows.

$$r = d(1+\cos\theta) \quad \text{where } d = \frac{(1+v)^2 K_{\mathrm{I}}^2}{9\pi\Sigma_{\mathrm{m}}^2} \tag{18}$$

A contour plot (a bigger solid line plot) of the hydrostatic stress and a circle which crosses the same intersections on the x- and y-axes are shown in Fig. 7. It is easy to prove that the diameter of the circle is equal to $2.5d$. Since in the early stage of ductile fracture a crack grows in a stable manner, the contour plot of a hydrostatic stress grows and advances (a small contour grows with the tip stably moving along the crack line, and it becomes a bigger contour) as shown in Fig. 7. Thus, the edge of the contour plot becomes almost circular like the cavitation zone observed in experiments. This implies that rubber particles cavitate at a constant hydrostatic stress. The hydrostatic stress causing cavitation can be easily obtained from Eq. (18) with $2.5d = 1600$ μm and $K_{\mathrm{I}} = 2.1$ MPa $\sqrt{\mathrm{m}}$, and it is 22.3 MPa.

3.3. Material constants for the hydrostatic stress-controlled void nucleation model

Any void nucleation model of the normal distribution function type has three material constants to be determined: the volume fraction of void nucleating particles such as rubber particles in the rubber-modified epoxy, the mean value and the standard deviation. It is easy to determine the volume fraction of void nucleating particles, but it is not so easy to determine the other two constants. Thus, in many researches using one of the void nucleation models the mean value and the standard deviation were somewhat arbitrarily determined (e.g., Chu and Needleman, 1980; Pan et al., 1983; Jeong and Pan, 1995, 1996). However, in this paper the two constants were determined by comparing simulation results with experimental results in terms of the size of the cavitation zone and the plastic zone. It would be possible to measure the void volume fraction at the edge of the cavitation zone by taking a detailed microscopy, but here it was assumed to be 0.005. If the mean value and the standard deviation are determined in such a way that the probability of the normal distribution function from 0 to 22.3 MPa is close to 0.042, the volume fraction of nucleated voids will be close to 0.005 ($= 0.042 \times f_{\mathrm{N}}$) when the hydrostatic stress reaches 22.3 MPa. Five sets of the mean value and the standard deviation resulting in the probability of 0.042 were used in the material behavior analyses around the crack tip under Mode I plane strain conditions; the five sets

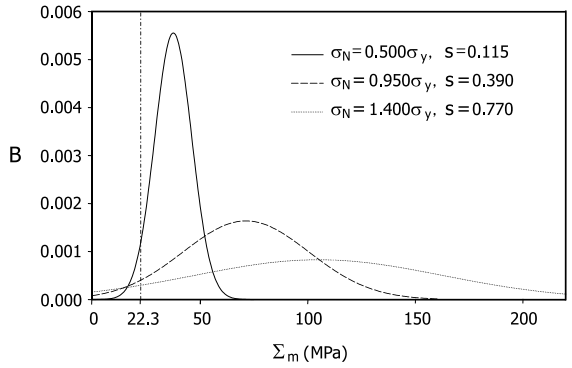

Fig. 8. Normal distribution functions for the hydrostatic stress-controlled void nucleation model.

were $\sigma_N = 0.500\sigma_y$, $s = 0.115$; $\sigma_N = 0.725\sigma_y$, $s = 0.250$; $\sigma_N = 0.950\sigma_y$, $s = 0.390$; $\sigma_N = 1.175\sigma_y$, $s = 0.565$ and $\sigma_N = 1.400\sigma_y$, $s = 0.770$. The normal distribution functions in Eq. (13) with the first, third and last sets were plotted in Fig. 8, and note that the area under each curve from 0 to 22.3 MPa is close to 0.005.

From the numerical simulations the void volume fraction f and the effective plastic strain E^p of the rubber-modified epoxy were obtained when the crack opening displacement (COD) became about three times the original COD. The contour plots of the void volume fraction are shown at the upper half, and the contour plots of the equivalent plastic strain are shown at the lower half in Fig. 9 with the coordinates normalized by $(K_I/\sigma_y)^2$. Due to symmetry, the contour plots of the void volume fraction or the equivalent plastic strain at the other half can be obtained by reflecting the contour plots with respect to the x-axis. Note that when the COD becomes over 2.5 times the original COD, steady state solutions usually arise, and the contour plots remain almost unchanged except within the area about a COD distance from a crack tip (McMeeking, 1977). The normalized diameter of the cavitation zone and the normalized length of the plastic zone observed in the experiment (Pearson and Yee, 1991) were 2.04 and 0.77, respectively. However, the numerical simulation with $\sigma_N = 0.500\sigma_y$, $s = 0.115$ resulted in the normalized diameter of the cavitation zone of 2.20 and the normalized length of the plastic zone of 0.87 as shown in Fig. 9(a). Even though the mean value and the standard deviation were determined to result in the normalized size of the cavitation zone of 2.04, the cavitation zone became slightly bigger because of void growth after nucleation. As shown in Fig. 8, with this set of the mean value and the standard deviation, voids were supposed to nucleate at relatively low hydrostatic stresses. Thus, nucleated voids grew in a large amount, and this was the reason why in the simulation the cavitation zone became bigger than it was supposed to be, and the massive cavitation zone (defined in this paper as a zone with $f \geqslant 0.0525$) became quite large. In addition, the plastic zone obtained in this simulation is longer than that observed in the experiment. The numerical simulation with $\sigma_N = 0.950\sigma_y$, $s = 0.390$ resulted in the normalized diameter of the cavitation zone of 2.05 and the normalized length of the plastic zone of 0.76 as shown in Fig. 9(b). The size and the shape of the massive cavitation zone are similar to those of the plastic zone. It is noteworthy that the size and the shape of the cavitation zone and the plastic zone obtained in this simulation are in good agreement with those obtained in the experiment. The numerical simulation with $\sigma_N = 1.400\sigma_y$, $s = 0.770$ resulted in the normalized diameter of the cavitation zone of 2.03 and the normalized length of the plastic zone of 0.62 as shown in Fig. 9(c). In this case, the size of the cavitation zone is very close to that of the experimental result, but the size of the plastic zone is smaller than that of the experimental result.

For the sake of brevity, the contour plots for $\sigma_N = 0.725\sigma_y$, $s = 0.250$ and $\sigma_N = 1.175\sigma_y$, $s = 0.565$ are not shown. However, the normalized diameters obtained from the simulations are 2.18 and 2.04, and the normalized lengths are 0.86 and 0.68, respectively. Therefore, it can be said that as the mean value (or the

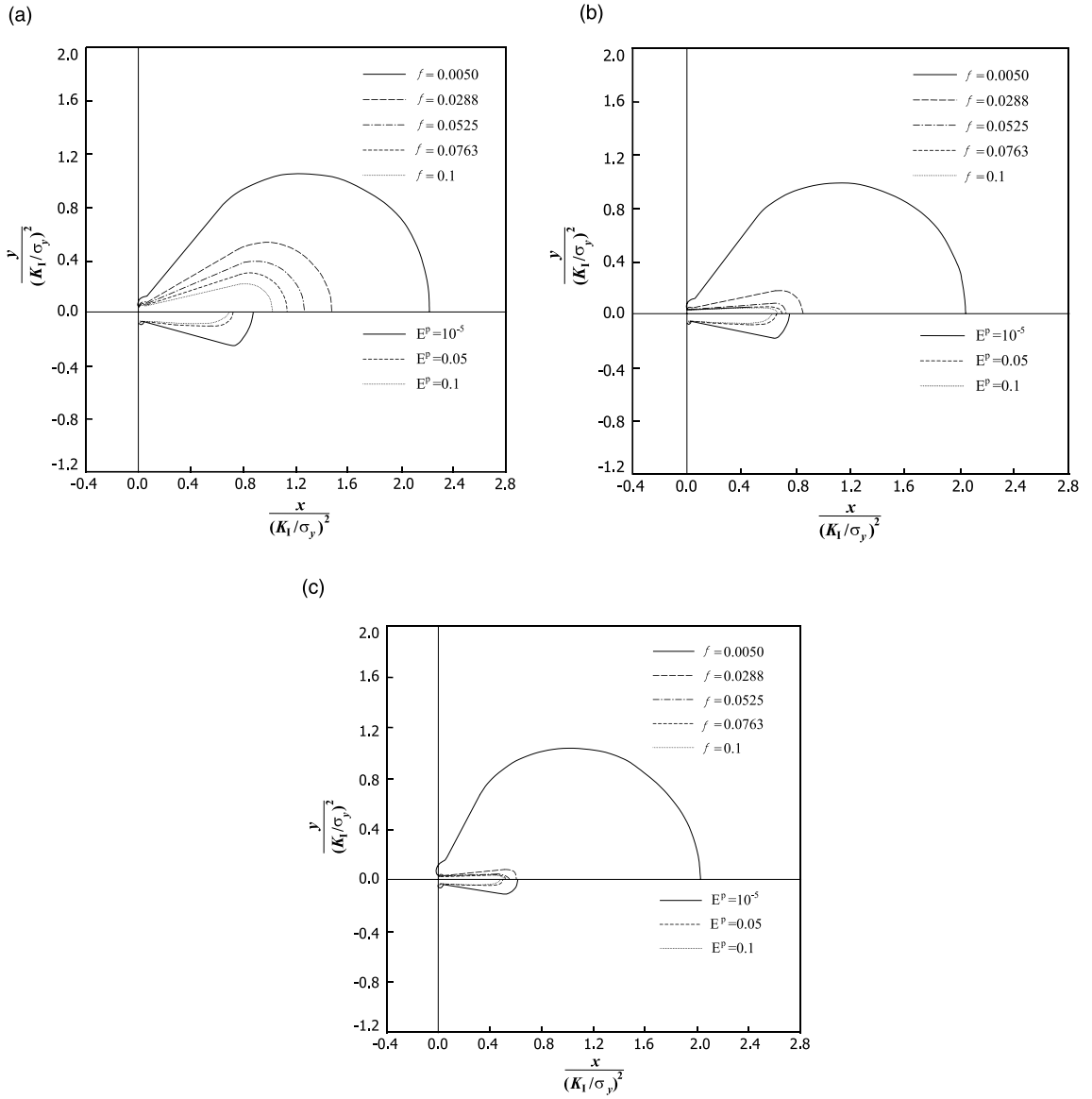

Fig. 9. (a) The contour plots of the void volume fraction and the effective plastic strain around the crack tip when the hydrostatic stress-controlled void nucleation model with $\sigma_N = 0.500\sigma_y$, $s = 0.115$ is used. (b) The contour plots of the void volume fraction and the effective plastic strain around the crack tip when the hydrostatic stress-controlled void nucleation model with $\sigma_N = 0.950\sigma_y$, $s = 0.390$ is used. (c) The contour plots of the void volume fraction and the effective plastic strain around the crack tip when the hydrostatic stress-controlled void nucleation model with $\sigma_N = 1.400\sigma_y$, $s = 0.770$ is used.

standard deviation) increases, the size of the cavitation zone and the plastic zone decreases. By comparing the size of the cavitation zone and the length of the plastic zone obtained in the simulations with those observed in the experiment, it can be concluded that the mean value and the standard deviation for the hydrostatic stress-controlled void nucleation model should be $\sigma_N = 0.950\sigma_y$, $s = 0.390$ to properly model the cavitation process occurring in the rubber-modified epoxy.

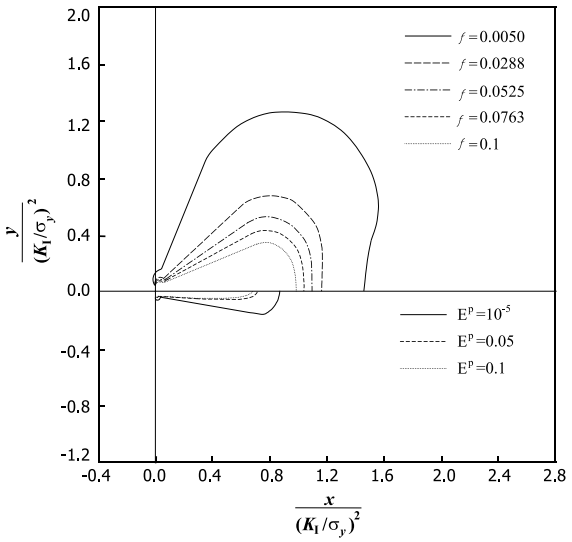

Fig. 10. The contour plots of the void volume fraction and the effective plastic strain around the crack tip when the maximum stress-controlled void nucleation model with $\sigma_N = 1.000\sigma_y$, $s = 0.225$ is used.

For the sake of comparison, the material behavior around the crack tip was also analyzed with the maximum stress-controlled void nucleation model used. The mean value and the standard deviation for the nucleation model were selected as $\sigma_N = 1.000\sigma_y$, $s = 0.225$ with no certain reason. The contour plots obtained from the simulation were shown in Fig. 10. The plastic zone formed along the crack line, and the cavitation zone surrounded the plastic zone as in the case of the hydrostatic stress-controlled void nucleation model used. However, the cavitation zone was not circular, but bigger along the y-axis as Jeong and Pan (1996) had already pointed out. The material behavior was also analyzed with the plastic strain-controlled void nucleation model used. However, in this case the cavitation zone became almost the same as the plastic zone, which was a lot smaller than the cavitation zone observed in the experiment. This is another piece of evidence that rubber particles in the rubber-modified epoxy started to cavitate before noticeable plastic deformation. Therefore, it is not appropriate to use either the maximum stress-controlled void nucleation model or the plastic strain-controlled void nucleation model in the material behavior analysis of the rubber-modified epoxy.

3.4. Material behavior around the notch tips

Al-Abduljabbar and Pan (1999) analyzed the material behavior of the rubber-modified epoxy in the SDEDN specimen under four-point bending, which had been experimentally investigated by Yee et al. (1993). Al-Abduljabbar and Pan (1999) assumed the rubber-modified epoxy to be a porous material from the beginning of deformation with no consideration of the cavitation process, and they showed circular contour plots of the hydrostatic stress around a notch under tension. However, in this paper the cavitation process was regarded as void nucleation process, which was modeled by using the hydrostatic stress-controlled void nucleation model with the mean value and the standard deviation determined in the previous section.

The contour plots of the void volume fraction and the effective plastic strain were obtained from the simulation when the crosshead moved downward by 1.6 mm. As shown in Fig. 11(a), a circular cavitation zone formed only around the lower notch, and the diameter of the cavitation zone was about 3 mm. In

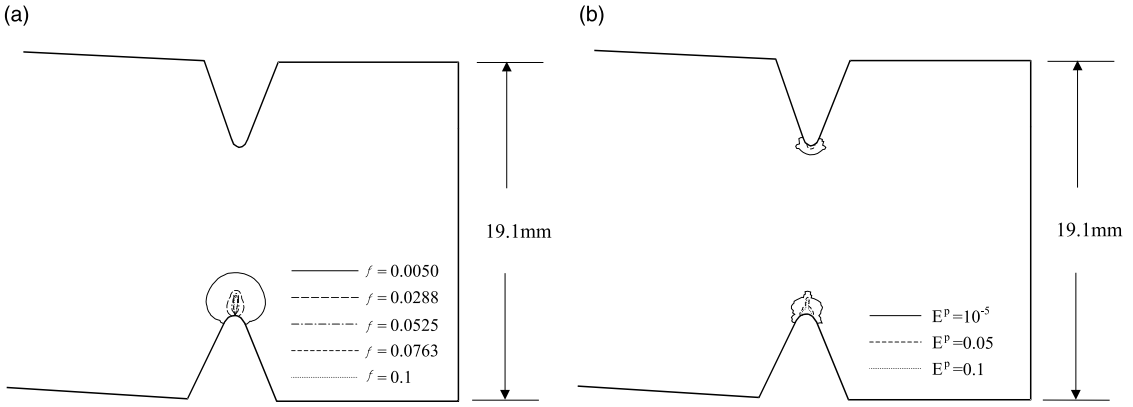

Fig. 11. (a) The contour plots of the void volume fraction in the SDEDN specimen. (b) The contour plots of the effective plastic strain in the SDEDN specimen.

contrast, no cavitation occurred around the upper notch because the material around it was under the negative hydrostatic stress throughout the deformation history. Note that inside the circular cavitation zone a massive cavitation zone formed along the vertical direction. As shown in Fig. 11(b), the plastic zone around the upper notch was smaller than that around the lower notch. Especially, the zone of $E^{p} \geqslant 0.05$ was quite small around the upper notch, but the zone was comparatively large around the lower notch, forming along the vertical direction. Experimental results showed that a circular cavitation zone occurred only around the lower notch, and inside the cavitation zone a plastic zone (or a massive cavitation zone) formed along the vertical direction (see Fig. 8(e) in Yee et al. (1993)). The experimental results also showed that the diameter of the cavitation zone was about 3 mm when the crosshead moved downward about 1.6 mm, and the plastic zone around the upper notch was quite small. Therefore, the simulation results are in good agreement with the experimental results, and the constitutive relations, especially the new yield function and the hydrostatic stress-controlled void nucleation model seem to be reasonable.

4. Conclusions

The new yield function developed in this paper is valid for porous solids with pressure-sensitive matrices under the negative hydrostatic stress as well as under the positive hydrostatic stress. When the void volume fraction is zero, the yield function becomes equal to Coulomb's yield function. When the matrix is pressure-insensitive, the yield function becomes equal to Gurson's yield function, three correction parameters being ignored. The yield function and the hydrostatic stress-controlled void nucleation model along with other constitutive relations were used to simulate the material behavior of a rubber-modified epoxy. The hydrostatic stress-controlled void nucleation model was used to mathematically represent the cavitation process occurring in a rubber-modified epoxy only under the positive hydrostatic stress.

Comparing the cavitation zone observed in an experiment with the contour plots of the hydrostatic stress around a crack in a rubber-modified epoxy (DER331/Pip/CTBN-8(10)) under the Mode I plane strain small-scale yielding conditions, the hydrostatic stress causing cavitation was determined, and it was 22.3 MPa. Five sets of the mean value and the standard deviation for the hydrostatic stress-controlled void nucleation model were determined in a way that the void volume fraction would become 0.005 when the hydrostatic stress changed from 0 to 22.3 MPa. They were used to analyze the cavitation and the plastic deformation around a crack in the rubber-modified epoxy. As the mean value increases along with the

standard deviation, the size of the cavitation zone and the plastic zone (and the massive cavitation zone) decreases. By comparing the numerical results with the experimental results, a set of the mean value and the standard deviation which resulted in almost the same size and shape of the cavitation zone and the plastic zone could be selected.

The same set was used to analyze the material behavior of the rubber-modified epoxy around the double notches in the SDEDN specimen under four-point bending. From this numerical simulation, a limited size of the plastic zone was obtained around the notch under compression, and a bigger circular cavitation zone with a massive cavitation zone formed inside of it was obtained around the notch under tension. It is noteworthy that the size and the shape of the cavitation zone around the notch under tension obtained from the numerical analysis were in agreement with those obtained from the experiment.

Al-Abduljabbar and Pan (1999) took no cavitation into account in their linear yield function for the negative hydrostatic stress. However, in this paper the author took into account the cavitation process by using the hydrostatic stress-controlled void nucleation model, which does not result in any void nucleation under the negative hydrostatic stress. Three correction parameters being ignored, the yield function proposed in this paper becomes equal to Coulomb's yield function when there are no voids. Therefore, both approaches are qualitatively the same except that cavitation zones could be obtained in the analyses of this paper. However, both approaches will produce quite different results in a material behavior analysis of a rubber-modified epoxy under cyclic loading. Suppose the SDEDN specimen shown in Fig. 4 is loaded in the opposite direction after the crosshead moved down by 1.6 mm. When the material around the lower notch is under compression, the material will have further plastic deformation even under the hydrostatic pressure due to cavitated rubber particles if the yield function proposed in this paper is used. However, the material will not have further plastic deformation under the hydrostatic pressure if the yield function proposed by Al-Abduljabbar and Pan (1999) is used. When the material has further plastic deformation under compression, the cavitated rubber particles will close up. This reduction of the void volume fraction can be taken into account by Eq. (11) because $\mathrm{tr}(\mathbf{D}^{\mathrm{p}})$ is negative and so is $\dot{f}$. Note again that the FEM results shown in Fig. 2 clearly show that a porous solid, in this case a rubber-modified epoxy with cavitated rubber particles, yields under the hydrostatic pressure. Therefore, for the cyclic loading case it is more appropriate to use the yield function proposed in this paper than the yield function proposed by Al-Abduljabbar and Pan (1999). In the future, the material behavior of a rubber-modified epoxy under cyclic loading will be analyzed.

Acknowledgements

The financial support for this work by Korea Research Foundation Grant (KRF-99-003-E00041) is highly appreciated. The valuable advice from Prof. Jwo Pan at the University of Michigan is also highly appreciated.

References

Al-Abduljabbar, A., Pan, J., 1999. Numerical analysis of notch-tip fields in rubber-modified epoxies. Polymer Engineering and Science 39, 662–675.

Argon, A.S., Im, J., 1975. Separation of second phase particles in spheroidized 1045 steel, Cu–0.6pct Cr alloy, and maraging steel in plastic straining. Metallurgical Transactions A 6, 839–851.

Bowden, P.B., 1973. The yield behavior of glassy polymers. In: Haward, R.N. (Ed.), The Physics of Glassy Polymers. Wiley, New York, pp. 279–339.

Chen, I.-W., 1991. Model of transformation toughening in brittle materials. Journal of American Ceramic Society 74, 2564–2572.

Chu, C.-C., Needleman, A., 1980. Void nucleation effects in biaxially stretched sheets. Transactions of the ASME 102, 249–256.

Gurson, A.L., 1975. Plastic flow and fracture behavior of ductile materials incorporating void nucleation, growth and interaction, Ph.D. thesis, Brown University.

Gurson, A.L., 1977. Continuum theory of ductile rupture by void growth. Part I. Yield criteria and flow rules for porous ductile media. Journal of Engineering Materials Technology 99, 2–15.

Haward, R.N., 1973. The post-yield behavior of amorphous plastics. In: Haward, R.N. (Ed.), The Physics of Glassy Polymers. Wiley, New York, pp. 340–393.

Kinloch, A.J., Young, R.J., 1983. Fracture Behavior of Polymers. Elsevier Applied Science, New York.

Kody, S.R., Lesser, A.J., 1998. Evaluation of yield criteria and energy absorbing mechanisms of rubber modified epoxies in multiaxial stress states, ANTEC 1998, 1448–1452.

Jeong, H.-Y., 1992. A macroscopic constitutive law for porous solids with pressure-sensitive matrices and its implications for plastic flow localization and crack-tip behavior, Ph.D. thesis, The University of Michigan, Ann Arbor.

Jeong, H.-Y., Pan, J., 1995. A macroscopic constitutive law for porous solids with pressure-sensitive matrices and its implications to plastic flow localization. International Journal of Solids Structure 32, 3669–3691.

Jeong, H.-Y., Pan, J., 1996. Crack-tip fields for porous solids with pressure-sensitive matrices and for rubber-modified epoxies. Polymer Engineering and Science 36, 2306–2319.

Lazzeri, A., Bucknall, C.B., 1993. Dilatational bands in rubber toughened polymers. Journal of Materials Science 28, 6799–6808.

Lazzeri, A., Bucknall, C.B., 2000. Recent developments in the modeling of dilatational yielding in toughened plastics. In: Pearson, R., Sue, H.-Y., Yee, A. (Eds.), Toughening of Plastics—Advances in Modelling and Experiments. Oxford University Press, Oxford, pp. 14–35.

McMeeking, R.M., 1977. Finite deformation analysis of crack tip opening in elastic–plastic materials and implications for fracture. Journal of the Mechanics and Physics of Solids 25, 357–381.

Needleman, A., Tvergaard, V., 1987. An analysis of ductile rupture modes at a crack tip. Journal of the Mechanics and Physics of Solids 35, 151–183.

Pan, J., Saje, M., Needleman, A., 1983. Localization of deformation in rate sensitive porous plastic solids. International Journal of Fracture 21, 261–278.

Pearson, R.A., Yee, A.F., 1986. Toughening mechanisms in elastomer-modified epoxies. Part 2. Microscopic studies. Journal of Materials Science 21, 2475–2488.

Pearson, R.A., Yee, A.F., 1991. Influence of particle size and particle size distribution on toughening mechanisms in rubber-modified epoxies. Journal of Materials Science 26, 3828–3844.

Rabinowitz, S., Ward, I.M., Perry, J.S.C., 1970. The effect of hydrostatic pressure on the shear yield behavior of polymers. Journal of Materials Science 5, 29–39.

Sauer, J.A., Pae, K.D., Bhateja, S.K., 1973. Influence of pressure on yield and fracture in polymers. Journal of Macromolecular Science—Physics B 8, 631–654.

Spitzig, W.A., Richmond, O., 1979. Effect of hydrostatic pressure on the deformation behavior of polyethylene and polycarbonate in tension and compression. Polymer Engineering and Science 19, 1129–1139.

Spitzig, W.A., Sober, R.J., Richmond, O., 1975. Pressure dependence of yielding and associated volume expansion in tempered martensite. Acta Metallurgica 19, 1129–1139.

Spitzig, W.A., Sober, R.J., Richmond, O., 1976. The effect of hydrostatic pressure on the deformation behavior of maraging and HY-80 steels and its implications for plasticity theory. Metallurgical Transactions A 7, 1703–1710.

Sternstein, S.S., Ongchin, L., 1969. Yield criteria for plastic deformation of glassy high polymers in general stress fields. American Chemistry Society Polymer (preprint) 10, 1117–1124.

Tandon, G.P., Weng, G.J., 1988. A theory of particle-reinforced plasticity. Journal of the Applied Mechanics 55, 126–135.

Tvergaard, V., 1981. Influence of voids on shear band instabilities under plane strain conditions. International Journal of Fracture 17, 389–407.

Tvergaard, V., 1982a. On localization in ductile materials containing spherical voids. International Journal of Fracture 18, 237–252.

Tvergaard, V., 1982b. Influence of void nucleation on ductile shear fracture at a free surface. Journal of the Mechanics and Physics of Solids 30, 399–425.

Yee, A.F., Pearson, R.A., 1986. Toughening mechanisms in elastomer-modified epoxies. Part 1. Mechanical studies. Journal of Materials Science 21, 2462–2474.

Yee, A.F., Li, D., Li, X., 1993. The importance of constraint relief caused by rubber cavitation in the toughening of epoxy. Journal of Materials Science 28, 6392–6398.

Yu, C.-S., Shetty, D., 1989. Transformation zone shape, size, and crack-growth–resistance [*R*-curve] behavior of ceria-partially-stabilized zirconia polycrystals. Journal of American Ceramic Society 72, 921–928.